Photon-echo attenuation in rare-earth-ion-doped crystals

S. B. Altner, G. Zumofen, and U. P. Wild
Physical Chemistry Laboratory, ETH-Zentrum, CH-8092 Zürich, Switzerland

M. Mitsunaga
NTT Basic Research Laboratories, Atsugi, Kanagawa 243-01, Japan
(Received 20 November 1995; revised manuscript received 15 August 1996)

We study the optical properties of rare-earth-ion-doped inorganic crystals with an emphasis on the dependence of two-pulse photon echoes on the excitation density in the system. The experimental investigations concentrate on Pr^{3+}:Nd^{3+}:Eu^{3+} codoped Y_2SiO_5 and $YAlO_3$ crystals at low temperatures. With two pulses of one laser the echo is induced in one ion species and with a third, ''scrambler'' pulse of a second laser another species is excited. These scrambler excitations lead to a dephasing and thus to an echo attenuation which depends on the strength, frequency, and time of the scrambler pulse. The spectral sensitivity of the echo attenuation is used for a spectroscopic technique: ''photon-echo attenuation spectroscopy.'' As a function of the delay time t_s between the scrambler pulse and the onset of the two-pulse echo sequence the attenuation shows a very specific behavior dictated by the excitation-induced frequency shifts (EFS's). For t_s between the two echo-inducing pulses the echo intensity is partially regained by the ''dephasing-rephasing balancing'' of the reversible EFS's. For the theoretical description a stochastic model is introduced and the dephasing by excitation-induced lattice vibrations and by EFS's are analyzed in detail. The present results are discussed in the light of previous experimental and theoretical investigations. [S0163-1829(96)05247-2]

I. INTRODUCTION

Photon-echo measurements have been intensively applied to study coherent optical phenomena in many materials. While at the beginning of these studies the experiments were designed to investigate the nature of the coherence, recently photon echoes have been used to gain information about the physical properties of the system hosting the echo generating species. Because the coherence is very sensitive to fluctuations in the environment photon echoes can be used for the investigation of weak effects, such as dynamical processes resulting from the ubiquitous ''two-level systems'' (TLS's).[1–10] A particular role in these investigations is played by rare-earth-ion-doped inorganic crystals; their optical properties are very appropriate for the study of various dephasing mechanism. The high optical frequency selectivity of these crystals, which can be of the order of kHz, combined with the high frequency resolution of the time domain techniques have rendered possible the study of phenomena not amenable by other techniques.[11–24]

Very small perturbations in the environment of a dopant-ion lead to changes in its transition frequency which in turn cause a dephasing in the excitation strong enough for detection. These perturbations may arise from stationary thermally activated processes, such as lattice vibrations or spin flips of magnetic compounds in the crystal. However, also the excitations involved in the echo inducing process give rise to a phase randomization. For example, the local electrostatic and magnetic fields at a probe ion are modulated by the excitation of neighboring ions. This induces an additional, nonthermal dephasing that depends on the excitation density, i.e., on the ion concentration, the oscillator strength, and the laser-pulse intensity.

In ''pure'' two-pulse photon-echo experiments, the excitation density can be varied by changing the concentration of the species participating in the echo process or by changing the laser intensity. For instance, Cooper, Olson, and Fayer[25] measured the echo-decay rate as a function of impurity concentration in mixed molecular crystals. Similarly, the echo intensity depending on the frequency position within the inhomogeneously broadened band was investigated by Shelby and Macfarlane.[11] Alternatively, experiments were carried out in which the intensities of the two pulses relative to each other were varied.[12–14] It was found that the behavior of the echo intensity decay changes dramatically when the first or second pulse was chosen to be strong; also nonexponential decay was observed. Both effects were interpreted as resulting from excitation-induced frequency shifts.

More recently, the two-pulse photon-echo experiments were extended by adding a third, scrambler pulse.[12,13,15,16] In these experiments the frequency of the scrambler pulse was positioned in the same transition band[12,13] or scanned over the resonances of another impurity species.[15,16] By the variation of the intensity, the frequency, and the delay time t_s between the scrambler pulse relative to the echo-pulse sequence several experimental parameters are at disposal. The technique of bichromatic optical excitations is similar to the photon-echo nuclear double-resonance (PENDOR) technique introduced by Hu, Leigh, and Hartmann.[26] This technique is the optical analog of the spin-echo ENDOR and consists of monitoring the photon-echo intensity as a function of an applied rf field with the frequency tuned over neighboring ion resonances[26] or over sublevels of the probe ions.[27]

The interpretation of the observed excitation-density dependent dephasing is primarily based on excitation-induced frequency shifts (EFS's). Frequency shifts were considered in the analysis of PENDOR resulting from nuclear transitions in the vicinity of the optically active species; for

pure optical experiments EFS's were first taken into account by Taylor and Hessler.[28] EFS's originate from the changes of the electrostatic properties of a species when excited. Consequently, the field in the vicinity of that species is changed and in turn this field change induces a Stark effect in another guest species; the corresponding shift in the transition frequency leads to a dephasing. This interpretation is strongly supported by the observation of dephasing resulting from an externally applied voltage.[19,20] The electric field induces Stark shifts in the transition frequencies and these shifts modulate the echo intensity. The two effects, EFS's and Stark shift, differ in field-strength distribution: for EFS's the field at a probe species is random due to the randomness in the environment while for an applied voltage the electric field is homogeneous in the system.

Basically, EFS's result from the diagonal interactions between the guest species which contrast with the off-diagonal, resonance interactions.[29,30] The latter were considered in the analysis of the echo intensity as a function of the laser-frequency position within the inhomogeneously broadened band. The interplay between the diagonal and off-diagonal interactions in excitation density-dependent photon echoes has not been clarified so far. The shifts due to off-diagonal interaction depend on the difference between the echo frequency and the scrambler frequency. If the frequency difference is much larger than the resonance frequency the dephasing by resonance interaction can be disregarded.[30] If, however, the two frequencies are identical or close to each other the off-diagonal interactions may contribute to the excitation-induced dephasing. This has to be considered particularly in ''pure'' two-pulse photon-echo experiments.

Another mechanism, leading to an excitation density-dependent dephasing, originates from excitation-induced lattice vibrations (ELV's). The nonradiative decay of the electronic excitation is accompanied by the dissipation of large amounts of electronic energy into nonequilibrium phonons. Scattering processes of these phonons at electronically excited species induce a phase randomization. Reabsorption of nonequilibrium phonons were considered by Macfarlane and Meltzer[31] and phonon scattering was accounted for by Bai and Kachru[21] for the interpretation of their observations that the echo attenuation changes when the focus of the laser is varied.

In our experiments we concentrate on bichromatic measurements of two-pulse photon echoes in multiple rare-earth ion-doped crystals. With two lasers two different ion species are excited. With the first laser the photon echo of the probe ions (A ion) is triggered; with the pulse of the second laser another ion species (B ion) is excited. This pump-probe scheme allows for independent control of the two-pulse photon echoes and of the excitation-induced dephasing.[15] By choosing well-separated A- and B-ion transition frequencies the dephasing by resonance interaction is avoided. The technique with two lasers and two optically active species has been proposed as a novel type of time and frequency resolved spectroscopy, ''echo-demolition spectroscopy''[16] also termed ''photon-echo attenuation spectroscopy'' (PEAS);[17] basically it is a double-resonance type of spectroscopy.

Theoretically, Klauder and Anderson[2] in their seminal paper introduced a model for the analysis of several coherence phenomena on the basis of flipping TLS's. This model, also called the ''sudden-jump'' model has been extended especially for the study of dephasing in glassy environments.[3,5–10] The fluctuations are assumed to result from interactions between the species involved in the echo process and the TLS's randomly placed in the system. The TLS's are characterized by sudden jumps between the two states with specific rates which depend on the system parameters and on the temperature. This model was applied in the study of EFS's by representing the two states of the TLS's by the ground and excited state of the B ions.[17] The electronic transitions of the scrambler species are taken as stochastic events, i.e., the optical active species are excited stochastically according to the excitation probability and they remain excited until they suddenly relax to the ground state with a probability according to an exponential decay law. According to this approach the echo attenuation as a function of the delay t_s is characterized by a unique behavior which allows for an identification of the dephasing by EFS's. This behavior follows from a partial dephasing-rephasing balancing (DRB) which is a consequence of the reversibility of EFS's. In this paper we extend our previous experimental and theoretical considerations and show that the DRB is robust against various modifications of the model.

The paper is structured as follows. In Sec. II the model is reviewed and the two mechanisms, dephasing by EFS's and dephasing by nonequilibrium phonons, are studied. In Sec. III the frequency and time-resolved experimental results obtained from Pr^{3+}:Nd^{3+}:Eu^{3+} codoped Y_2SiO_5 and $YAlO_3$ crystals are presented and the corresponding spectroscopic data are tabulated. The results are discussed in Sec. IV with special attention to previous observations. Further theoretical results are given in the Appendix.

II. THE STOCHASTIC APPROACH

We assume that the system responsible for the echo process consists of an ensemble of noninteracting A ions. For an optically thin sample the echo intensity is

$$\mathcal{I}(t_{12},t_s)=|P(t_{12},t_s)|^2, \tag{1}$$

where, recalling, t_s denotes the time instance of the scrambler pulse relative to the time of the first pulse which is assumed to take place at time $t=0$. t_{12} is the pulse separation time and $P(t_{12},t_s)$ denotes the system polarization in the rotating-frame approximation[32,33]

$$P(t_{12},t_s)=-\tfrac{1}{2}ic\mu\,\sin(A_1)\sin^2(A_2/2)R_0(t_{12})R(t_{12},t_s), \tag{2}$$

A_j is the area of the jth excitation pulse and c is the concentration of the A ions. $R_0(t_{12})$ is the echo attenuation due to the excitation lifetimes and due to thermally activated processes. We introduced $R(t_{12},t_s)$ to describe the dephasing induced by the electronically excited neighborhood. It is supposed that the echo is recorded at the low excitation limit so that the density of the A-ion excitation does not significantly contribute to the total excitation density. We concentrate exclusively on the excitation-induced dephasing and thus on the reduced intensity,

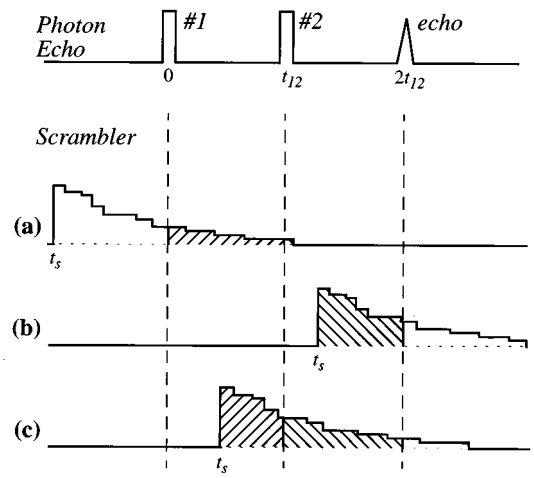

FIG. 1. Schematic illustration of the dephasing by EFS's for the three different cases discussed in the text. The lines, following staircases, denote $\omega_j(t)$ and depict the temporal relaxation of the EFS's. The shaded areas indicate the contributions to the phase shift; the areas of the rephasing period contribute with a negative sign. Dephasing-rephasing balancing can take place in case (c).

$$\frac{\mathcal{I}(t_{12},t_s)}{\mathcal{I}_0}=|R(t_{12},t_s)|^2, \tag{3}$$

where $\mathcal{I}_0$ is the echo intensity with the scrambler pulse shut off. $R(t_{12},t_s)$ is assumed to result from transition frequency fluctuations[2,32]

$$R(t_{12},t_s)=\left\langle \exp i\left[\int_0^{t_{12}}\omega_j(t)dt-\int_{t_{12}}^{2t_{12}}\omega_j(t)dt\right]\right\rangle, \tag{4}$$

where $\omega_j(t)$ is the transition frequency of the jth A ion with fluctuations resulting exclusively from the time-dependent shifts induced by the scrambler excitations.

Excitation-induced frequency shifts

We first study the dephasing by EFS's which results from the excited-state environment. For this process three situations are relevant: (a) If the scrambler pulse is applied at times t_s before the first echo pulse the EFS's are larger in the dephasing than in the rephasing period. (b) If t_s is located in the time range of the rephasing period only the rephasing process is perturbed; in both cases an echo attenuation results. (c) If, however, the time t_s is in the range of the dephasing period between the first and the second echo pulse, the phase perturbations in the dephasing and rephasing periods can be balanced; thus the echo intensity is partially regained. This is more obvious from Fig. 1 where the three situations (a) to (c) are schematically illustrated.

For the description of this process we make use of the previous analyses of the sudden-jump and related models.[2,6,7,9,17,34,35] We write for the time-dependent electronic transition frequency $\omega_j(t)$ of the jth A ion

$$\omega_j(t)=\omega_{j0}+\sum_k \epsilon_{jk}\xi_k u_k(t), \tag{5}$$

where the sum runs over all lattice sites of possible B-ion positions. ϵ_{jk} is the frequency shift of the A-ion transition induced by the excitation of a B ion at a displacement $\mathbf{r}_{jk}$; it is of the form[4,36]

$$\begin{aligned}\epsilon_{jk}=&\langle\phi^A_{je}\phi^B_{ke}|V_{jk}|\phi^A_{je}\phi^B_{ke}\rangle-\langle\phi^A_{je}\phi^B_{kg}|V_{jk}|\phi^A_{je}\phi^B_{kg}\rangle\\&-\langle\phi^A_{jg}\phi^B_{ke}|V_{jk}|\phi^A_{jg}\phi^B_{ke}\rangle+\langle\phi^A_{jg}\phi^B_{kg}|V_{jk}|\phi^A_{jg}\phi^B_{kg}\rangle,\end{aligned} \tag{6}$$

where ϕ denotes the wave functions of the A and B ions and where the indices g and e refer to ground and excited state, respectively. This expression describes the change in the A ion transition frequency caused by the B-ion excitation. The two center expansion in terms of electrostatic properties leads to multipolar interactions.

The $\xi_k u_k(t)$ term in Eq. (5) is introduced to account explicitly for the randomness of the spatial configuration and for the stochastic nature of the B-ion excitations. ξ_k is an indicator variable indicating whether the kth site is occupied by an excited B ion at time $t=t_s$,

$$P_\xi=\begin{cases}(1-p), & \xi=0\\ p, & \xi=1,\end{cases} \tag{7}$$

where p is the dimensionless excitation density in the system denoting the probability of a lattice site to be occupied by a B ion that is excited at time t_s. Accordingly, ξ takes the value 0 with probability $1-p$ and the value 1 with probability p. $u(t)$ gives the stochastic aspect of the model with the B-ion excitation initiated at t_s and surviving until time t_f, so that

$$u(t)=\begin{cases}1, & t_s<t<t_f\\ 0, & \text{otherwise.}\end{cases} \tag{8}$$

The decay time t_f is distributed according to the exponential probability density

$$P_{t_f}=\gamma e^{-\gamma(t_f-t_s)}, \tag{9}$$

with $\gamma=1/T_1^B$ as the decay rate defined above. Basic in this description is the independence of the B ions so that P_ξ and P_{t_f} apply independently to all possible lattice sites. Equations (5), (7)–(9) provide a clearly outlined model which allows for the calculation of the dephasing due to EFS's by averaging over spatial and temporal configurations.

This model was used to generate the EFS trajectories of Fig. 2. They were calculated for a cubic lattice and for dipolar interactions. For the initial time $t=0$ lattice sites k were chosen randomly within a sphere of 10^5 lattice sites according to the relative occupation probability $p=10^{-2}$. For these sites ξ_k was set to one and otherwise to zero. The EFS was then calculated from the sum over these sites $\Sigma_k\epsilon_{jk}\xi_k$. For each occupied site, $\xi_k=1$, a lifetime t_f was chosen randomly according to an exponential decay law with the rate γ. At these times the corresponding ξ_k were reset to zero. This procedure leads to the relaxing trajectories shown in the upper part of Fig. 2. In the lower part of the figure the EFS's are plotted as a function of $\exp(-\gamma t)$ to achieve a sequence of events according to a Poissonian distribution of occurrence. The corresponding pattern is typical for Cauchy random walks; the trajectories are characterized by jumps on

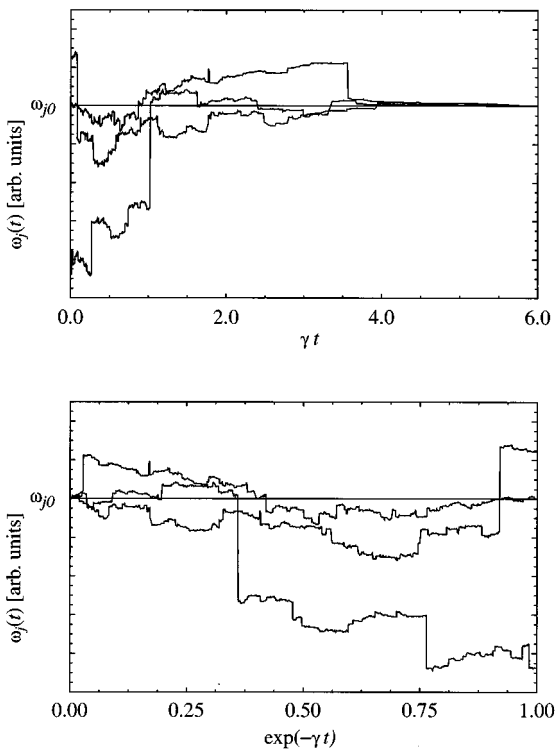

FIG. 2. Computer simulation of EFS's trajectories. Plotted are three realizations of time-dependent EFS's calculated from the procedure discussed in the text. In the upper figure the trajectories are plotted as a function of time, in the lower figure as a function of $e^{-\gamma t}$, respectively. The Cauchy random-walk characteristics and the self-affine property are evident.

many scales and by the self-affine property.[37] The pattern of these trajectories are very different from the schematic ones in Fig. 1. Although the trajectories in Fig. 2 indicate that perfect balancing of the accumulated phase has vanishing probability a partial balancing still appears feasible.

The accumulated phase of jth A ion is

$$\int_0^{t_{12}} \omega_j(t)dt - \int_{t_{12}}^{2t_{12}} \omega_j(t)dt = \sum_k \epsilon_{jk}\xi_k\theta_k(t_s), \quad (10)$$

where

$$\theta_k(t_s) = \int_0^{t_{12}} u_k(t)dt - \int_{t_{12}}^{2t_{12}} u_k(t)dt. \quad (11)$$

$\theta_k(t_s)$ is a random variable depending on the stochastic decay time t_f which enters through $u(t)$. We obtain

$$R(t_{12},t_s) = \left\langle \prod_k \exp(i\epsilon_{jk}\xi_k\theta_k(t_s)) \right\rangle_{\{\xi,t_f\}}, \quad (12)$$

where the average has to be taken over the initial B-ion excitation configurations and over the stochastic decay times. Accounting for the independence of P_ξ and P_{t_f} the averages can be taken over the individual lattice sites independently,

$$R(t_{12},t_s) = \prod_k \langle \exp(i\epsilon_{jk}\xi_k\theta_k(t_s)) \rangle_{(\xi,t_f)_k}. \quad (13)$$

The ξ average yields

$$R(t_{12},t_s) = \prod_k \{1 - p[1 - S_{jk}(t_s)]\}, \quad (14)$$

where

$$S_{jk}(t_s) = \langle \exp[i\epsilon_{jk}\theta(t_s)] \rangle_{t_f}. \quad (15)$$

$S_{jk}(t_s)$ is a quantity that was studied previously;[15] the explicit expression reads

$$S_{jk}(t_s) = \begin{cases} 1 + \dfrac{i\epsilon}{\gamma - i\epsilon} e^{\gamma t_s} + \dfrac{i\epsilon}{\gamma + i\epsilon} e^{\gamma(t_s - 2t_{12})} - \dfrac{2i\epsilon\gamma}{\gamma^2 + \epsilon^2} e^{\gamma(t_s - t_{12}) + i\epsilon t_{12}}, & t_s \leq 0 \\ \dfrac{\gamma}{\gamma - i\epsilon} + \dfrac{i\epsilon}{\gamma + i\epsilon} e^{\gamma(t_s - 2t_{12}) - i\epsilon t_s} - \dfrac{2i\epsilon\gamma}{\gamma^2 + \epsilon^2} e^{(\gamma - i\epsilon)(t_s - t_{12})}, & 0 < t_s \leq t_{12} \\ \dfrac{\gamma}{\gamma + i\epsilon} + \dfrac{i\epsilon}{\gamma + i\epsilon} e^{(\gamma + i\epsilon)(t_s - 2t_{12})}, & t_{12} < t_s \leq 2t_{12} \end{cases} \quad (16)$$

where $\epsilon = \epsilon_{jk}$. Equations (3), (14), and (16) represent an exact solution of the problem within the model assumptions; they can be applied for the detailed calculation of the echo attenuation for a particular lattice structure and interaction law. For small p expression (14) can be approximated by

$$R(t_{12},t_s) \simeq \exp\left\{ -p \sum_k \{1 - \langle \exp[i\epsilon_{jk}\theta(t_s)] \rangle_{t_f}\} \right\}. \quad (17)$$

We consider the multipolar description of the interaction potential. The dipole-dipole approximation gives

$$\epsilon_{jk} = \epsilon_0 (r_0/|\mathbf{r}_{jk}|)^3 \kappa(\Omega), \quad (18)$$

where ϵ_0 denotes the interaction of dipoles at a unit distance r_0 and depends on the differences between the dipoles of the excited and the ground state for the A and B ions, respectively, according to Eq. (6). Dielectric corrections to the dipolar interactions originating form the polarizable hosting environment are thought to be included in the constant ϵ_0. κ gives the angular dependence

$$\kappa(\Omega)=(\hat{d}_A,\hat{d}_B)-3(\hat{r},\hat{d}_A)(\hat{r},\hat{d}_B), \tag{19}$$

where $\hat{d}_{A,B}$ and $\hat{r}$ are unit vectors for the dipoles and the displacement, respectively. Ω denotes the set of angles defining the corresponding spatial orientations. Tacitly we have assumed that the orientation of the B-ion dipoles is the same for all sites. In the continuum approach Eq. (17) yields

$$\mathcal{R}\{\ln R(t_{12},t_s)\}\simeq-\left\langle 4\rho_0\pi p\int_0^\infty dr\ r^2\{1-\cos[\epsilon_0(r_0/r)^3\kappa\theta(t_s)]\}\right\rangle_{\Omega,t_f}=-C_1p\langle|\theta(t_s)|\rangle_{t_f}, \tag{20}$$

where ρ_0 denotes the site density. Only the real part is considered because the imaginary part cancels in Eq. (3). The constant in Eq. (20) is

$$C_1=(2/3)\pi^2\epsilon_0 r_0^3\rho_0\langle|\kappa|\rangle_\Omega. \tag{21}$$

The dimensionless quantity $\langle|\kappa|\rangle_\Omega$ is of the order 1. For the particular case with the A dipole parallel to the B dipoles we have $\langle|\kappa|\rangle_\parallel=4/\sqrt{27}$ and for the case of the A dipole perpendicular to the B dipoles $\langle|\kappa|\rangle_\perp=2/\pi$, respectively. The calculation of $\langle|\theta(t_s)|\rangle_{t_f}$ gives[17]

$$\gamma\langle|\theta(t_s)|\rangle_{t_f}=\begin{cases}(1-e^{-t_{12}\gamma})^2e^{t_s\gamma}, & t_s\leqslant 0\\ (2e^{-(2t_{12}-t_s)\gamma}-e^{-2t_{12}\gamma}-2e^{-t_{12}\gamma}+e^{-t_s\gamma})e^{t_s\gamma}, & 0<t_s\leqslant t_{12}\\ (1-e^{-(2t_{12}-t_s)\gamma}), & t_{12}<t_s\leqslant 2t_{12}.\end{cases} \tag{22}$$

From Eqs. (3), (20), and (22) the echo intensity depending on t_s exhibits a specific behavior, as shown in Fig. 3. For the time regimes $t_s<0$ and $t_{12}<t_s<2t_{12}$ the logarithm of the echo intensity follows a behavior dictated by one exponential. In the intermediate regime $0<t_s<t_{12}$, the behavior is more complicated; the echo intensity may show a local maximum $t_{s,\max}=\gamma^{-1}\ln[(1+2e^{t_{12}\gamma})/4]$, $t_{12}\gamma>\ln(3/2)$.[17] This maximum is a signature of the dephasing by EFS's.

In Fig. 4 the echo attenuation as a function of t_{12} is shown for two fixed t_s values: $t_s=0$ and $t_s=t_{12}$. A very different decay is observed for two cases. Setting $t_s=0$ and $t_s=t_{12}$ in Eq. (22) and expanding for small γt_{12}, we obtain $\ln[\mathcal{I}(t_{12},t_s=0)/\mathcal{I}_0]\sim-(\gamma t_{12})^2$ and $\ln[\mathcal{I}(t_{12},t_s=t_{12})/\mathcal{I}_0]\sim-\gamma t_{12}$. Thus the echo intensity follows approximately a Gaussian in the former and an exponential decay in latter case.

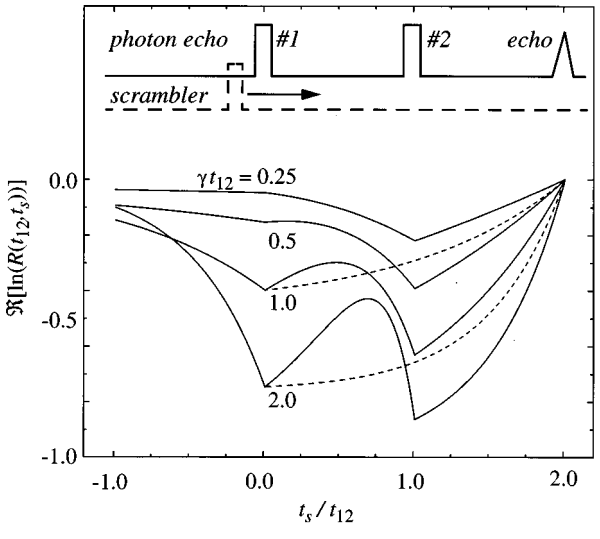

FIG. 3. Theoretical echo intensities as a function of the time delay t_s. The function $-C_1p\langle|\theta(t_s)|\rangle$ of Eq. (20) is given by full lines for various γt_{12} values as indicated and for $C_1p\gamma^{-1}=1$. To highlight the difference between the behaviors of the attenuation by to ELV's and EFS's, Eq. (26) is given by dashed lines with the value of $pD\gamma^{-1}$ chosen so that the corresponding full and dashed lines match for $t_s<0$ and for the cases of $\gamma t_{12}=1$ and 2.

Excitation-induced lattice vibrations

We now focus on the dephasing due to ELV's. We assume that part of the electronic energy is dissipated into lattice vibrations which may be highly excited localized vibrations or propagating phonons. Localized lattice vibrations

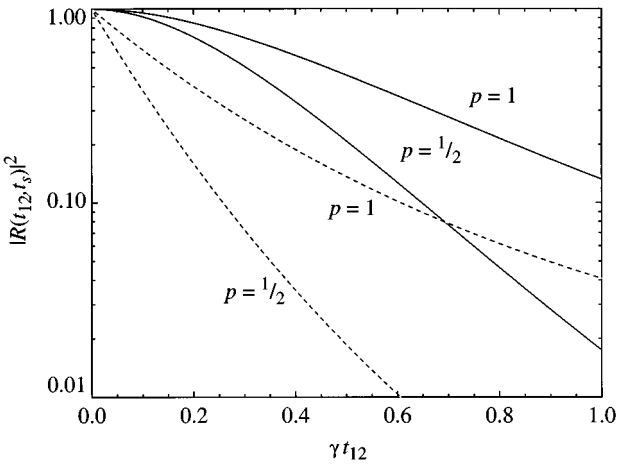

FIG. 4. Theoretical echo intensities as a function of the interpulse time t_{12}. Plotted is $\mathcal{I}(t_{12},t_s)/\mathcal{I}_0$ for $t_s=0$ as full lines and for $t_s=t_{12}$ as dashed lines, respectively, and for two p values, as indicated. The parameters are $\epsilon_0\rho_0r_0^3/\gamma=1$ and $\hat{d}_A\|\hat{d}_B$.

relax and eventually merge into propagating phonons. The dephasing is assumed to result from elastic- and inelastic-scattering processes of nonequilibrium phonons at electronically excited ions. A scattering event at an excited A ion is associated with a sudden frequency excursion giving rise to a dephasing. The efficiency of the dephasing depends on the frequency, the mean free path, and the lifetime of the phonons.[38] On one hand, we assume that the lifetime of the phonons until thermalization is short if compared with the electronic excitation lifetimes or dephasing times. Therefore the limiting process for the nonequilibrium phonon density is the electronic excitation decay and thus the nonequilibrium phonon density is proportional to the electronic excitation density. From this follows also, for example, that nonequilibrium phonons generated earlier than the first echo-inducing pulse do not lead to a significant dephasing and can be disregarded. On the other hand, it is supposed that the lifetime is sufficiently long so that scattering events with A-ion excitations are guaranteed.

Two different situations result from these assumptions: the scrambler pulse occurs before or after the first echo-inducing pulse. Relevant for the dephasing are the number of scattering events, i.e., the number of excitation dissipation events during the echo dephasing-rephasing process. For $t_s<0$ nonthermal lattice vibrations are generated during the whole dephasing-rephasing period $0<t<2t_{12}$ and the resulting echo attenuation depends only on the scrambler excitation density at time $t=0$. The situation is similar for $t_s>0$. Only the time period $2t_{12}-t_s$ enters the calculations. Thus by increasing t_s the echo attenuation is reduced. The scattering processes lead to a phase randomization irrespective of whether the polarization is in the dephasing or rephasing stage. Consequently, the strongest attenuation is expected to take place for $t_s=0$.

The dephasing by ELV's contrasts with the dephasing by EFS's. The energy excursions induced by phonon-scattering processes are fast relative to the coherence phenomena. Consequently, correlations between phonon-induced frequency fluctuations of the de- and rephasing period are negligible and a DRB can thus be ruled out. The experimental technique based on two species excitations provides fortuitous conditions for discriminating the competing effects.

For the description of this process we suppose unspecified nonequilibrium phonons and assume that the scattering events lead to frequency fluctuations $\Delta(t)$ which can be approximated by white noise. More explicitly, the fluctuations $\Delta(t)$ are δ correlated and Gaussian distributed so that

$$\langle\Delta(t)\rangle=0, \quad \langle\Delta(t)\Delta(t')\rangle=2\delta(t-t')pDe^{-\gamma(t-t_s)}, \tag{23}$$

where p has the same meaning as in Eq. (7). D is a constant and the exponential behavior accounts for the fact that the probability of the scattering events decays as the number density of surviving B-ion excitations. $\gamma=1/T_1^B$ is the decay rate which is considered to be identical for all B ions in the system. From a second cumulant expansion, we obtain

$$\ln R(t_{12},t_s)=-\tfrac{1}{2}K_2, \tag{24}$$

where

$$K_2=2pD\int_{\max(0,t_s)}^{2t_{12}} e^{-\gamma(t-t_s)}dt. \tag{25}$$

For the dephasing we find

$$\ln R(t_{12},t_s)=\begin{cases}-\gamma^{-1}pDe^{\gamma t_s}(1-e^{-2t_{12}}), & t_s<0\\ -\gamma^{-1}pD(1-e^{-\gamma(2t_{12}-t_s)}), & 0<t_s<2t_{12}\end{cases}. \tag{26}$$

For fixed t_{12} the behavior of $\ln R(t_{12},t_s)$ as a function of t_s is governed by one exponential both for $t_s<0$ and for $t_s>0$ and shows a minimum at $t_s=0$. Thus the attenuation is strongest for $t_s=0$ as we have anticipated. For fixed t_s and as function of t_{12} the expansion of the right-hand side (rhs) of Eq. (26) leads to an exponential decay of $R(t_{12},t_s)$ which holds for small γt_{12} values. This exponential decay is reminiscent of the decay due to the interaction with thermally activated processes which have been established to lead to exponential decays. Thus from this behavior no distinction between the thermally activated and excitation-induced effects can be made. However, by variations of temperature and excitation density a discrimination is possible. In Fig. 3 the echo attenuation by ELV's and EFS's are compared; the very different behavior is obvious from the presentation.

Dephasing by ELV's was reported in Ref. 21 and a similar interpretation was introduced for the electronic level repopulation by repeated resonant phonon emission and absorption in Ref. 31. In our experimental investigations dephasing by ELV's could not be traced. We stress that the approximations introduced for modeling the ELV's may not hold strictly. Nevertheless, it is thought that the present description captures the main effect. Moreover, the introduction of ELV's is appropriate here, because ELV's can be considered as a representative of excitation-induced dephasing resulting from irreversible frequency shifts.

III. EXPERIMENTAL INVESTIGATIONS

The setup

The experimental setup, schematically depicted in Fig. 5, consists of a classical collinear photon-echo arrangement, and in addition, of a second, counterpropagating beam, acting as the scrambler. The cw output of an Ar^+-ion laser pumped Coherent-Radiation CR 699 single-mode dye laser was fed through a doublet of acousto-optic modulators (AOM's 1 and 2, Matsushita EFL 200) that produced pulses of 1.5-μs length. These pulses were used to induce photon echoes which were detected with a photomultiplier. A third AOM of the same type was used to prevent the detector from saturation by selective opening at the expected echo time. The peak intensities of the pulses were of the order kW/cm^2 and led to reasonably strong echoes. To minimize the perturbing effects of spectral hole burning, the laser was repetitively scanned over a range of 200 MHz within one second. The echo sequence was repeated at a rate of 100 Hz, averages were taken over several tens of sequences for one data point.

In the case of spectroscopic measurements a second laser, an Ar^+-ion laser pumped Spectra Physics 375B tunable linear dye laser, was used to induce the excited-state environment to be probed by the echo sequence of the first laser. The

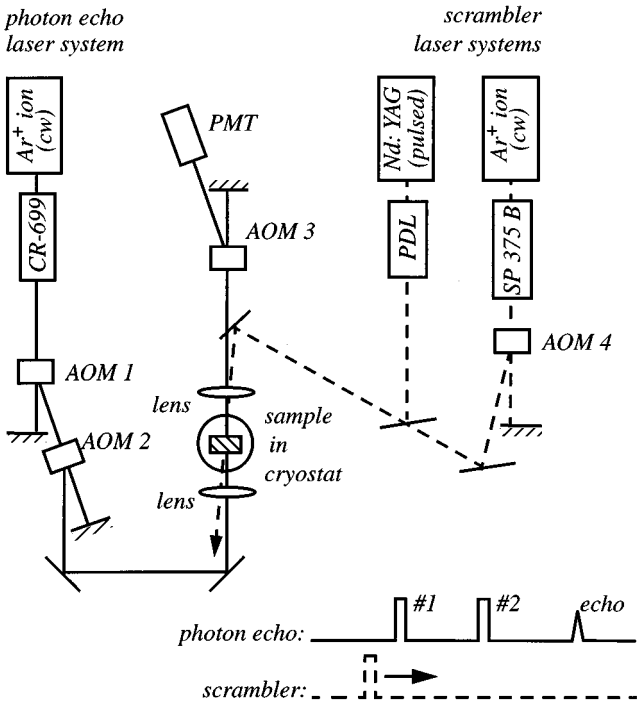

FIG. 5. Experimental setup for the echo-attenuation experiments. Depending on the type of the experiment, either the gated cw system or the pulsed system is used as the excitation-inducing light source. For clarity, the scrambler and the echo beams are not parallel to each other. AOM's denotes the acousto-optic modulator, PMT the photomultiplier tube, and PDL the pulsed dye laser, respectively.

scrambler laser with cw output power of 3 W was gated by a fourth AOM's to produce pulses of 10–100-μs duration. These pulses were sent through the crystal counterpropagating to the echo-inducing pulses. The overlap of the scrambler and echo laser beams was carefully optimized to induce a feasible echo attenuation. The spectral width of the scrambler laser was 40 GHz, which lead to an instrument limited resolution for some of the spectral features as is observed in the figures presented below. In the case of the DRB experiments a Spectra Physics/Quanta-Ray Nd:YAG DCR3 pumped-pulsed dye laser system PDL-2 was used, which generated pulses of kW power in bursts of approximately 4 ns. Thus the total scrambler energy was the same for both setups; however, the pulses were much shorter in the DRB experiments.

Y_2SiO_5 and $YAlO_3$ doped with rare-earth ions are known for their very long dephasing times since only very few magnetic compounds are present in these systems.[23,24] By spin flip flops these compounds give rise to a phase randomization. Owing to the small concentrations of these compounds the measurement of dephasing rates in the order of kHz is feasible. We used Eu^{3+}:Pr^{3+}:Nd^{3+} codoped Y_2SiO_5 and $YAlO_3$ crystals of 10-mm length. The concentrations of the dopants were nominally 0.1%, 0.01%, and 0.01%, respectively. The samples were held in an Oxford flow cryostat at temperatures of 6–7 K. At these temperatures thermally activated dephasing is negligible which is obvious from Fig. 6, where two-pulse photon-echo measurements of the homogeneous linewidths Γ_{hom} are displayed for Eu^{3+}:Y_2SiO_5 and for Eu^{3+}:$YAlO_3$. In this study we were interested only in the temperature dependence of the echo-decay rates; therefore the usual zero-intensity extrapolation and the application of static magnetic fields was omitted. In case of Y_2SiO_5 the onset of the thermally induced homogeneous line broadening takes place at 8 K. The data were fit to a T^7-Debye law which accounts for two-phonon Raman processes.[39,40] Good agreement with the experimental observations was obtained which makes sense because the electronic excited state involved in the echo process is clearly separated from neighboring electronic levels, so that a one-phonon-assisted depopulation cannot take place. The Debye temperatures of these crystals are unknown; thus it is not clear whether the difference in the rise of the linewidths with increasing temperature is because of different Debye temperatures or different electron-phonon couplings of the two systems. We conclude that for the interpretation of the echo-attenuation spectra recorded at 6–7 K thermally activated dephasing can be disregarded.

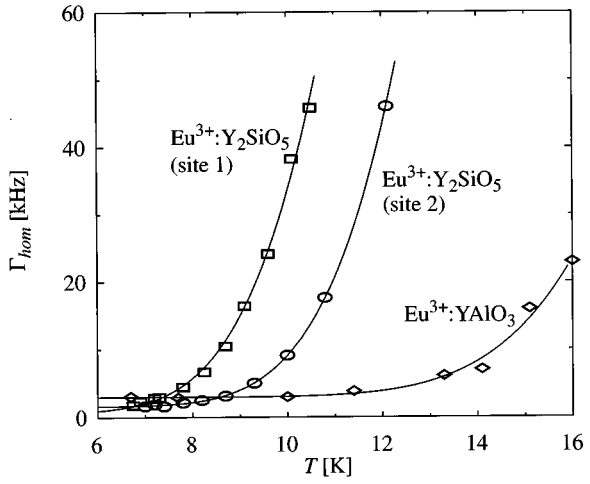

FIG. 6. Temperature dependence of the homogeneous linewidth Γ_{hom} of the Eu^{3+} $^7F_0-^5D_0$ transition measured by two-pulse photon echoes. The onset of the temperature dependence of the dephasing occurs at lower temperatures in the Y_2SiO_5 than in $YAlO_3$. The symbols give the experimental values and the full lines are fitted curves according to the T^7 law.

Experimental findings

We first report on the echo attenuation as a function of the scrambler wavelength. The echo-inducing laser was set onto the Pr^{3+} $^1D_2-^3H_4$ transition of Y_2SiO_5 and of $YAlO_3$ and onto the $^7F_0-^5D_0$ transition of Eu^{3+} site 1 in Y_2SiO_5 and of Eu^{3+} in $YAlO_3$. In parallel the scrambler laser was tuned over the range of 575–610-nm limited by the Rhodamine 6G laser dye. The scrambler pulses were of 100-μs duration and were triggered 100 μs (Y_2SiO_5) and 220 μs ($YAlO_3$) before the onset of the first echo pulse. The echo intensity was recorded as a function of the scrambler frequency; the corresponding spectra for Y_2SiO_5 and $YAlO_3$ are shown in Figs. 7 and 8, respectively. The traces show that the echo attenuation is strong for resonances between the scrambler frequency and the transition frequencies of the codoped species

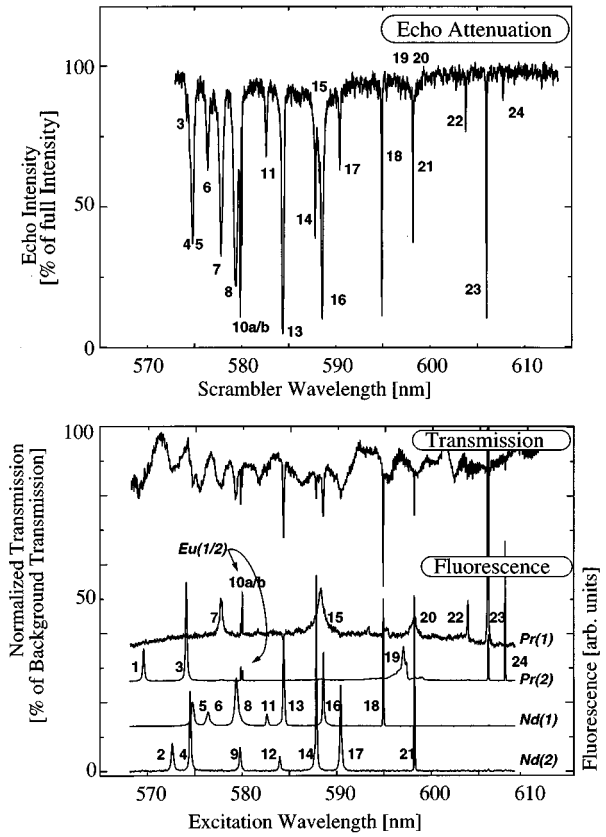

FIG. 7. Comparison of echo-attenuation, transmission, and fluorescence excitation spectra obtained from Pr^{3+}:Nd^{3+}:Eu^{3+} codoped Y_2SiO_5 crystals. The echo-attenuation spectrum of the upper box was recorded with the echo laser tuned onto the Eu^{3+} $^7F_0-^5D_0$ transition of site 1. Transmission and fluorescence excitation spectra are shown in the lower box. The spectral features are numbered ascendantly with increasing wavelength; corresponding resonance wavelengths and excited-state lifetimes are listed in Table I.

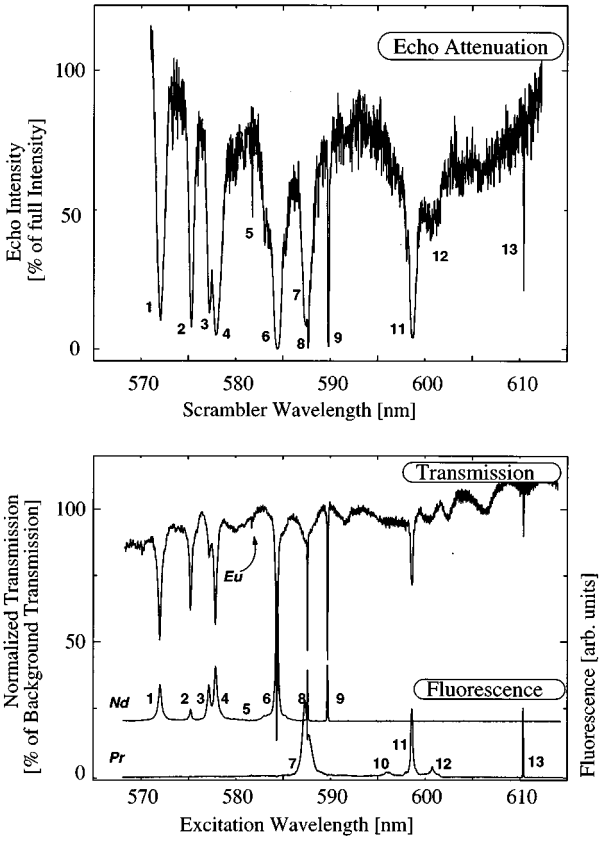

FIG. 8. Same as Fig. 7 but for spectra obtained from Pr^{3+}:Nd^{3+}:Eu^{3+} codoped $YAlO_3$ crystals with the echo laser in resonance with the Eu^{3+} $^7F_0-^5D_0$ transition. Corresponding spectral and temporal data are listed in Table II.

and the attenuation is absent where none of these species absorbs, independent of the frequency gap between scrambler and echo-inducing laser. These observations clearly support the interpretation in terms of nonresonant excitation-induced dephasing.

For comparison the transmission and fluorescence excitation spectra are also presented in Figs. 7 and 8; they confirm the observations by PEAS. All three types of spectra were recorded with approximately the same experimental parameters of the lasers which were used to induce the scrambling and the fluorescence, and to probe the transmission. With regard of the signal-to-noise ratio, the echo-attenuation spectra turn out to be superior to the transmission spectra but not quite as noiseless as the fluorescence excitation spectra. In the latter case, different detectors had to be used because of the different frequency ranges of the codoped ion emissions. Further, a monochromator (Nikon, P250) and lock-in amplification (Stanford Research SR850 DSP) were used to discriminate the emissions of different species. Such refinements in the detection procedure are not necessary in the echo-attenuation experiment, since it is always the photon echo of the same transition which is monitored whereas the spectral selectivity enters by a second perturbing mechanism.

The measured transition wavelengths of the Eu^{3+}:Pr^{3+}:Nd^{3+} codoped Y_2SiO_5 and $YAlO_3$ are summarized in Tables I and II. The accuracy of the wavelength measurements was limited by the poor frequency calibration of the linear dye laser. The spectra were recorded as a function of the position of a steppermotor which was driving a frequency tuning etalon. The position values were then transformed into wavelength units using a calibration based on known transition wavelengths of Eu^{3+}, Nd^{3+}, and Pr^{3+} $YAlO_3$,[41–43] the estimated accuracy is 0.1–0.2 nm. The transition wavelengths of the Y_2SiO_5 dopings observed in this study were previously reported except those of Nd^{3+}. Within the given accuracy the wavelengths presented in the tables for Pr^{3+} and Eu^{3+} are in agreement with the values reported in Refs. 24, 44.

Because several experimental parameters can be varied freely, there is no *standard* photon-echo-attenuation spectrum and the declaration of the applied parameters is an integral part of the spectrum. This is illustrated in Fig. 9 where spectra are shown for two different delay times t_s. The two traces represent portions of the Y_2SiO_5 attenuation spectrum, analogous to the one given in Fig. 7. The echo laser was tuned to the Eu^{3+} site 1 transition and the interpulse time was $t_{12}=150$ μs. The lower trace was recorded for $t_s=100$ μs and the upper spectrum for $t_s=1000$ μs. Notably, in the latter case only the long-living Eu^{3+} excitations contribute to the echo attenuation whereas the excitation of the other codoped species has disappeared.

TABLE I. Compilation of spectroscopic data for the Pr^{3+}:Nd^{3+}:Eu^{3+}:Y_2SiO_5 crystal measured by PEAS and by absorption and fluorescence spectroscopy. The relative errors, given in parentheses in the last column, are calculated from rms values for transitions with the same upper electronic states.

Species	Transition	Vacuum wavelength[a] (nm) (line number in Fig. 7)	Fluorescence lifetime T_1[b] (ms) (previously reported values[a])	Excited-state lifetime T_1 (ms) by echo attenuation and rel. error
Eu (site 1)	$^7F_0$–$^5D_0$	580.0 (10a)	1.87 (1.9)	1.67 (8%)
Eu (site 1)		580.2 (10b)	1.58 (1.6)	1.43 (6%)
Pr (site 1)	$^3H_4$–$^1D_2$	578.1 (7), 588.0 (15), 597.8 (20), 603.7 (22), 605.9 (23)	0.16 (0.16)	0.18 (9%)
Pr (site 2)		570.8 (1), 574.8 (3), 596.7 (19), 607.9 (24)	0.21 (0.22)	0.20 (6.5%)[c]
Nd (site 1)	$^4I_{9/2}$–$^4G_{5/2}+^2G_{7/2}$	575.4 (5), 576.9 (6), 579.6 (8), 582.6 (11), 584.3 (13), 588.3 (16), 594.6 (18)	0.25 (−)	0.26 (6.5%)
Nd (site 2)		573.5 (2), 575.2 (4), 580.0 (9), 583.9 (12), 587.6 (14), 590.1 (17), 597.9 (21)	0.33 (−)	0.33 (5%)[d]

[a]For comparison see Refs. 22 and 49.
[b]Mean value of all lines.
[c]Lines 1 and 3 do not show enough scrambling.
[d]Lines 4, 5, and 9 are burried by Nd (site 1) lines.

We now focus on the echo attenuation as a function of the delay t_s. In Fig. 10 we present experimental results obtained for Pr^{3+} and Nd^{3+} in Y_2SiO_5 and for four different scrambler pulse lengths. These results are compared with the predictions of Eqs. (20)–(22); good agreement is obtained in all cases. According to the predictions the temporal behavior of the echo intensity as a function of t_s in the regime $t_s<0$ follows an exp-exp law with the rate equal to $\gamma=(T_1^B)^{-1}$. The lifetimes fitted to the four data sets were the same within the accuracy of the measurements. For most of the strong resonances such time-resolved measurements have been carried out. The fitted lifetimes are summarized in Tables I and II together with corresponding lifetimes obtained from fluorescence excitation measurements. We notice a good agreement between the two sets of data. With the PEAS method one is thus able to distinguish between different species by means of their excited-state lifetimes. The lifetime of a non-frequency selective species is also given in Table II. This species was observed only for the $YAlO_3$ crystal; its lifetime is similar to the other listed values, its origin, however, is unclear.

From Eqs. (20)–(22) and from Fig. 4 it is obvious that for $t_s<0$ the observed excitation density dependent attenuation cannot be attributed either to EFS's or to ELV's processes. Therefore we focused on the regime $0<t_s<2t_{12}$. To assure quasi-instantaneous scrambling excitation, the high-power pulsed dye laser instead of the gated cw laser was used in these experiments. The experimental results were presented in Fig. 3 of Ref. 17. The echo intensity recovery was found to reach a maximum at 80 ± 5 μs for all laser intensities, in

TABLE II. Same as Table I, except for the Pr^{3+}:Nd^{3+}:Eu^{3+}:$YAlO_3$ crystal.

Species	Transition	Vacuum wavelength[a] (nm) (line number in Fig. 8)	Fluorescence lifetime T_1[b] (ms) (previously reported values[a])	Excited-state lifetime T_1 (ms) by echo attenuation and rel. error
Eu	$^7F_0$–$^5D_0$	581.7 (5)	1.77 (2.0)	not enough line strength
Pr	$^3H_4$–$^1D_2$	587.4 (7), 595.8 (10), 598.4 (11), 600.6 (12), 610.7 (13)	0.17 (0.18)	0.18 (9%)
Nd	$^4I_{9/2}$–$^4G_{5/2}+^2G_{7/2}$	573.0 (1), 575.8 (2), 577.6 (3), 578.2 (4), 584.3 (8), 587.2 (8), 589.5 (9)	0.18 (0.18)	0.19 (7%)
Unknown		nonselective		0.24 (7%)

[a]For a comparison see Refs. 17, 46, 47, 48.
[b]Mean value of all lines.

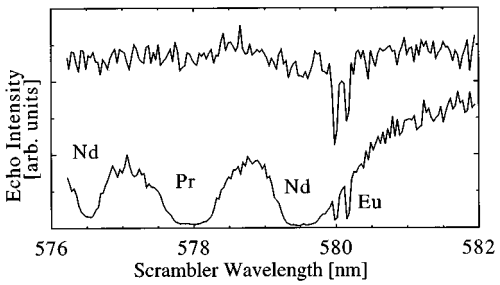

FIG. 9. Temporal selectivity of the echo-attenuation spectroscopy. The intensity is plotted for the echo induced in the $^7F_0-^5D_0$ transition of Eu^{3+} site 1 in Y_2SiO_5 for different values of the delay time t_s. Lower trace for $t_s=100$ μs: all codoped species are visible; upper trace for $t_s=1000$ μs: only the transitions of the long-living Eu^{3+} excitations of the two sites are visible.

agreement with the prediction of 79 μs obtained for $t_{12}=200$ μs and $\gamma^{-1}=T_1^{\mathrm{Nd}}=245$ μs. Also the scaling properties were examined and a reasonable data collapse on a single master curve was observed.

IV. DISCUSSION

The combination of careful measurements and theoretical developments allow now for an accurate detection and description of the excitation density-dependent photon-echo attenuation in rare-earth ion-doped inorganic crystals. The dephasing by excitation-induced frequency shifts manifests itself extraordinarily by the dephasing-rephasing balancing; the observation of this effect indicates very strongly the echo attenuation by excitation-induced frequency shifts. It can be detected by choosing appropriate transitions of the echo inducing and of the scrambler species. By means of the PEAS quantitative spectral information about the guest species and

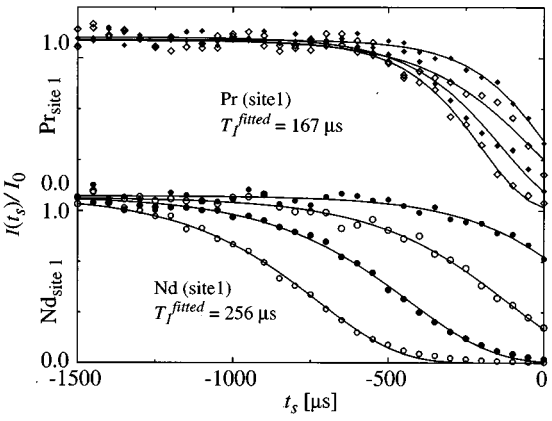

FIG. 10. Excitation-induced echo attenuation for $t_s<0$. The echoes were generated for the $^7F_0-^5D_0$ transition of Eu^{3+}-site 1 in Y_2SiO_5. The upper traces give the attenuation with the scrambler laser tuned onto the Pr^{3+}-site 1 transition at 605.81 nm (line Nr. 23 in Fig. 7) and the lower traces with the scrambler laser tuned onto the Nd^{3+}-site 1 transition at 584.40 nm (line Nr. 13 in Fig. 7). The scrambler pulse lengths were from top to bottom 7, 13, 25, and 100 μs. The fitted T_1 values are the same within the experimental errors.

about the system can be obtained.

Because of the time and frequency analogy additional verification of the EFS's can be achieved by the measurement of the excitation density-dependent line broadening. In experiments under current considerations a spectral hole is burnt into the transition of one species and is examined subject to a strong scrambler excitation density in the system. This technique is expected to provide independently the parameter $2C_1p$ as obtained from echo-attenuation measurements. To calculate $2C_1p$ from first principles further information about the guest species and the host system is required. C_1 depends on the dipole-moment differences of the two species involved, on the dielectric corrections, and on the geometric arrangement of the guest species in the system. p depends on the transition probability and the concentration of the scrambler species. By independent experiments based on Stark shifts induced by an applied electric field the dipole-moment differences and their geometry in the crystal can be determined.[45] Together with data from dielectric and fluorescence measurements the *a priori* calculation of the parameter $2C_1p$ appears feasible.

Our theoretical considerations are based on a stochastic approach for the description of the scrambler excitations. It leads to a surprisingly accurate description of the observed echo attenuation. The extension of the derivations to three-pulse stimulated photon echoes plus scrambling is straightforward. The approach of the present work is similar to that of the sudden-jump model based on TLS's, which oscillate stochastically between their two possible states. Accounting for all possible realizations of jump sequences between the two states makes a statistical analysis cumbersome. The situation is simpler in the present model where the scrambler excitations play the role of TLS's which can change their states only twice: excitation and deexcitation. The derivation of analytical expressions is thus facilitated.

In our study we compared the echo attenuation by ELV's and by EFS's to each other. Our experimental findings could be interpreted on the basis of EFS's exclusively. However, we point out that for $t_s<0$ we cannot discriminate between the two effects because they lead to identical behaviors. In order to distinguish between the two contributions the t_s range has to be extended to positive values. Bai and Kachru concluded from their experiment on ion-doped inorganic crystals that propagating nonequilibrium phonons are essentially responsible for the dephasing at strong excitation density.[21] We believe that this conclusion could be corroborated by experiments with two different guest species combined with variations of the laser foci.

From our analysis we are able to comment on the two-pulse laser experiments with a strong first or second pulse. Disregarding for a moment the resonance interaction, in a rough approximation we may assume that the strong pulse is identical to the scrambler pulse and that the weak pulse induces the echo at the low-intensity limit. Strong first or second pulse correspond to the two cases $t_s=0$ and $t_s=t_{12}$ as considered in Fig. 4. This approximation allows for the analysis of the echo intensity in terms of Eqs. (20)–(22). The observed nonexponential in the former and the fast exponential echo decay in the latter case, respectively are thus evident.[12–14]

At this instance the question arises of how the resonance

interaction comes into play in two-pulse photon echoes.[30] Disregarding the phonon-assisted energy-level repopulation, the echo attenuation by resonance interaction depends crucially on the difference between the transition frequencies of the interacting species. Therefore, the echo attenuation by resonance interaction depends on the energy-level density at the frequency position of the echo. Consequently, supposing a constant excitation density induced by the laser pulses, the dephasing by resonance interaction is a function of the frequency position within the inhomogeneously broadened band, which is contrary to the dephasing by EFS's. Roughly, the dephasing depends solely on the excitation density in the system and, again supposing a constant excitation density, the frequency position within the inhomogeneously broadened band is of no importance. While the interpretation of experimental echo intensities in terms of EFS's is straightforward, the analysis in terms of resonance interaction seems to be complicated; further theoretical and experimental investigations are required to shed light on this problem.

ACKNOWLEDGMENTS

We thank Dr. P. Neu for helpful discussions and Dr. Takahei for providing us with a pulsed dye laser. The support by the ''Swiss Priority Program: Optical Sciences, Applications, and Technology'' is gratefully acknowledged. One of us (S.B.A.) thanks NTT for the hospitality during the time when part of this work was carried out.

APPENDIXES

In these Appendixes, we present further theoretical results on excitation-induced frequency shifts relevant for future experimental investigations. We begin with the question of how many B ions contribute typically to the echo attenuation.

APPENDIX A: NUMBER OF INTERACTING IONS

We consider Eq. (16) noticing that the behavior of the rhs as a function of ϵ shows a crossover at $\gamma=\epsilon$. Thus one is able to distinguish between close and distant B ions by defining a characteristic radius $(R_c/r_0)^3=\epsilon_0/\gamma$.[5] We also introduce an outer radius R_n which spans a sphere of n lattice sites. Making use of Eq. (20), we find

$$\mathcal{R}\{\ln R(t_{12},t_s)\} \simeq -4\pi\rho_0 p\left[\int_{R_{\min}}^{R_c} r^2\,dr + \frac{1}{2}\,\epsilon_0^2\langle\theta^2(t_s)\rangle\langle\kappa^2\rangle r_0^6\int_{R_c}^{R_n} dr\; r^{-4}\right], \tag{A1}$$

where $R_{\min}$ is the smallest possible distance to a B ion. The first term is obtained by observing that for large arguments the cosine function in Eq. (20) oscillates rapidly as a function of r, so that its contribution can be disregarded. The second term results from the second-order expansion. Integration yields

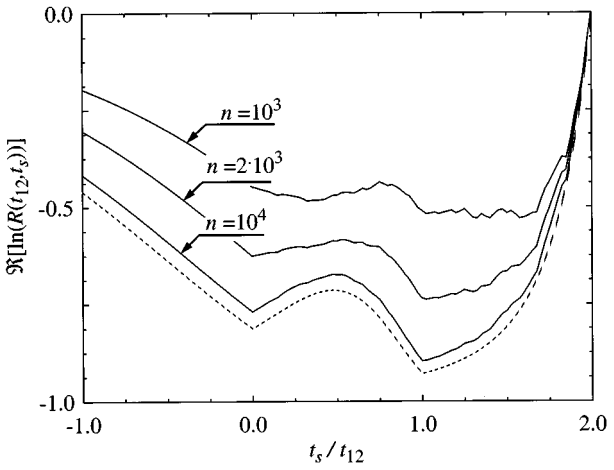

FIG. 11. Convergence of the echo attenuation with increasing number n of lattice sites to the asymptotic limit. The full lines give the result of Eq. (14) with the product restricted to the n-nearest sites, where the n values are as indicated. The dashed line is the asymptotic limit according to Eqs. (20)–(22). Further parameters are set: $p=10^{-3}$, $\epsilon_0/\gamma=10^3$, $\hat{d}_A\perp\hat{d}_B$, and $\gamma t_{12}=1$.

$$\mathcal{R}\{\ln R(t_{12},t_s)\} \simeq -\frac{4\pi}{3}\,\rho_0 p\left[R_c^3-R_{\min}^3+\frac{1}{2}\,r_0^6\epsilon_0^2\langle\theta^2(t_s)\rangle\langle\kappa^2\rangle \times(R_c^{-3}-R_n^{-3})\right]. \tag{A2}$$

We note that for experimentally typical situations with $\epsilon_0/\gamma\gg1$ and accounting for $(4\pi/3)\rho_0 R_{\min}^3\simeq1$ the correction resulting from the lower integration limit $R_{\min}$ is small. Therefore the lower integration limit set to zero in Eq. (20) is a reasonable approximation. Alternatively, we may write

$$\begin{aligned}\mathcal{R}\{\ln R(t_{12},t_s)\} &\simeq -4\pi\rho_0 p\left[\int_0^\infty\cdots-\int_{R_n}^\infty\cdots\right]\\ &\simeq -p\left[C_1\langle|\theta(t_s)|\rangle-\frac{2\pi}{3}\,\rho_0 r_0^6\epsilon_0^2\langle\kappa^2\rangle\langle\theta^2(t_s)\rangle R_n^{-3}\right].\end{aligned} \tag{A3}$$

Equating $(4\pi/3)\rho_0 R_n^3=n$, we see that Eqs. (A2) and (A3) converge with an increasing number of sites as $1/n$. We estimate the number N of excited B ions from $N=pn$. Only a finite number of excitations contribute significantly to the attenuation. Nevertheless, Eqs. (A2) and (A3) also make clear that the question of how many B-ion excitations contribute to the attenuation cannot be strictly answered; this number depends on the percentage of the attenuation to be covered by the estimate, on the parameters and on the details of the model. In Fig. 11 we present the relative echo intensity as a function of t_s for various numbers n. The curves demonstrate the convergence towards the asymptotic result.

APPENDIX B: EXCITATION-INDUCED LINE BROADENING

Usually the relationship between the time and frequency domain experiments is pointed out. Here we are interested in the analogy between the echo attenuation and the line broadening due to EFS's. Because of the finite lifetime of the scrambler excitations the line broadening is transient.

We first wish to comment on the instantaneous spectral diffusion which results from $\Sigma_k \epsilon_{jk}\xi_k u_k(t)$ in Eq. (5). This sum represents a random frequency due to the randomness of indicator variables ξ_k and due to the stochastic property of $u(t)$. In order to obtain statistical insight into the EFS's and its time evolution we may reason as follows.[46] For small excited B-ion densities p one may consider the above sum as to be a sum of independent and equally distributed variables. This is more obvious if the terms in the sum are thought to have been assembled randomly. The distribution of the variables follows from the spatial dependence of the interaction and from the spatial density of the B ions. Considering $|\epsilon(r)| \sim r^{-3}$ for dipolar interactions and $P(r) \sim r^2$ for the spatial probability density of the B-ion excitations, we obtain for the jump probability distribution

$$P(\epsilon) \sim |\epsilon|^{-2}, \quad |\epsilon| \leq \epsilon_{\max}. \tag{B1}$$

We note that this corresponds to the asymptotic behavior of a Lorentzian. Together with the idea of randomly and equally distributed variables the calculation of the sum is reminiscent of random walks with a structure function based on the Lorentzian distribution. The corresponding evolution is termed Lévy flights[47,48] or ''Lorentzian diffusion.'' [2] In Eq. (B1) the power-law behavior of $P(\epsilon)$ is limited to the range $|\epsilon| \leq \epsilon_{\max}$, where $\epsilon_{\max}$ is due to the smallest possible displacement to a neighboring site.

Although the line broadening has been studied for the sudden-jump model,[49] we repeat the derivations to highlight the parallelism between the time and frequency domain description. For the shape $P(\omega,t)$ of the time-dependent line broadening we write

$$P(\tilde{\omega},t) = \left\langle \delta\left[\tilde{\omega} - \sum_k{}' \ \epsilon_{jk}\xi_k u_k(t) \right] \right\rangle_{\{\xi, t_f\}}, \tag{B2}$$

where we have set $\tilde{\omega} = \omega - \omega_{j0}$. In Fourier ($\tilde{\omega} \to z$) space the configuration average can be carried out; we obtain

$$P(z,t) = \prod_k \ \{1 - p e^{-(t-t_s)\gamma}[1 - \exp(i\epsilon_{jk} z)]\}, \tag{B3}$$

which is analogous to Eq. (14) of the corresponding dephasing process. For small p, dipolar interactions, and the continuum description we find

$$\begin{aligned} \ln P(z,t) &\simeq -4\pi\rho_0 p e^{-(t-t_s)\gamma} \\ &\quad \times \int_0^\infty dr \ r^2 \left\{ 1 - \left\langle \exp\left[i\epsilon_0 \left(\frac{r_0}{r} \right)^3 \kappa z \right] \right\rangle_\Omega \right\} \\ &= -p e^{-(t-t_s)\gamma}[C_1 |z| + i C_2 z], \end{aligned} \tag{B4}$$

where C_1 is the constant of Eq. (21) and where

$$C_2 = -(2/3)\pi\epsilon_0\rho_0 r_0^3 \left\langle \int_0^\infty dx \ x^{-2} \sin(\kappa(\Omega)x) \right\rangle_\Omega. \tag{B5}$$

For $\hat{d}_A \perp \hat{d}_B$ one has $C_2 = 0$, while for $\hat{d}_A \| \hat{d}_B$ the integration is involved[50]

$$C_2 = -\frac{4\pi^2 \epsilon_0 \rho_0 r_0^3}{9\sqrt{3}} \left[\sqrt{3} + \ln \frac{1-\sqrt{3}}{1+\sqrt{3}} \right] \simeq -0.66 \epsilon_0 \rho_0 r_0^3. \tag{B6}$$

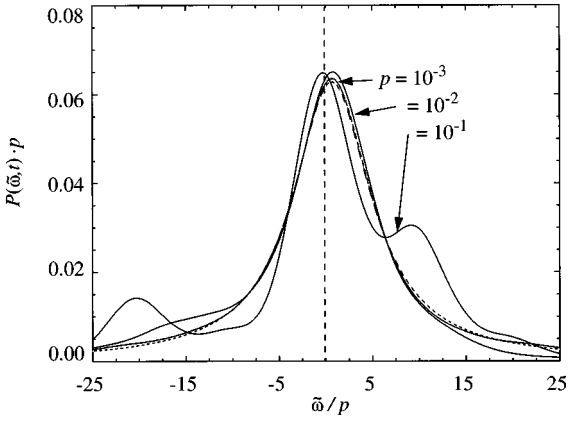

FIG. 12. Line broadening due to EFS's. $P(\tilde{\omega},t)$ calculated from Eq. (B3) is plotted in the rescaled representation as full lines for several p values, as indicated and for $t = t_s$, a cubic lattice, $\hat{d}_A \| \hat{d}_B$, $\epsilon_0 \rho_0 r_0^3/\gamma = 1$. The asymptotic form according to Eq. (B4) is given as a dashed line.

In frequency space expression (B4) corresponds to a Lorentzian with a width of $2C_1 p e^{-(t-t_s)\gamma}$ and is centered at $-C_2 p e^{-(t-t_s)\gamma}$. It follows that the broadening relaxes exponentially while the specific shape is time invariant. Figure 12 shows the line shape calculated numerically from the Fourier back transform of Eq. (B3) for various occupation probabilities p. For larger p values the particular pattern in the lineshape results form the discrete structure of the lattice. This pattern disappears with decreasing p and the shape converges to the asymptotic limit with the center shifted according to Eq. (B4).

APPENDIX C: NONDIPOLAR INTERACTIONS

We now investigate how the specific behavior of the echo attenuation depends on the interaction range. We consider higher-order multipolar interactions,

$$|\epsilon| \sim c r^{-s}, \tag{C1}$$

where s denotes the range of interaction; for $s = 3$ we recover the dipolar situation. We disregard the angular dependence which is complicated and not of relevance here. Analogous to Eq. (17), we have

$$\begin{aligned} &\mathcal{R}\{\ln R(t_{12}, t_s)\} \\ &\quad \simeq \left\langle -4\pi\rho_0 p \int_0^\infty dr \ r^2 \{1 - \cos[c r^{-s} \theta(t_s)]\} \right\rangle_{t_f}. \end{aligned} \tag{C2}$$

Integration yields

$$\mathcal{R}\{\ln R(t_{12}, t_s)\} \simeq -C_\beta p \langle |\theta(t_s)|^\beta \rangle_{t_f}, \tag{C3}$$

where we introduced $\beta = 3/s$ and where the constant reads $C_\beta = (2/3)\pi^2 \rho_0 c^\beta \csc(\beta\pi/2)/\Gamma(\beta)$, which for $\beta = 1$ and $c = \epsilon_0$ reproduces C_1 of Eq. (21). We also find

$$\gamma^{\beta}\langle|\theta(t_s)|^{\beta}\rangle_{t_f}=\begin{cases} e^{t_s\gamma}\tilde{\gamma}(1+\beta,t_{12}\gamma)+e^{-(2t_{12}-t_s)\gamma}\tilde{\gamma}(1+\beta,-t_{12}\gamma), & t_s\leq 0 \\ \tilde{\gamma}[1+\beta,\gamma(t_{12}-t_s)]+(\gamma t_s)^{\beta}e^{-(2t_{12}-t_s)\gamma} & \\ \quad +e^{-2(t_{12}-t_s)\gamma}\{\tilde{\gamma}[1+\beta,-\gamma(t_{12}-t_s)]+\tilde{\gamma}(1+\beta,\gamma t_s)\}, & 0<t_s\leq t_{12} \\ \gamma^{\beta}(2t_{12}-t_s)^{\beta}e^{-(2t_{12}-t_s)\gamma}+\tilde{\gamma}[1+\beta,\gamma(2t_{12}-t_s)], & t_{12}<t_s\leq 2t_{12}, \end{cases} \tag{C4}$$

where $\tilde{\gamma}(\beta,x)$ stands for the incomplete gamma function, $\tilde{\gamma}(\beta,x)=\int_0^x e^{-t}t^{\beta-1}dt$ and for negative arguments, $\tilde{\gamma}(\beta,-x)=\int_0^x e^{t}t^{\beta-1}dt$, respectively.[51] The behavior of R as a function of t_{12} or of t_s is not obvious from Eq. (C4). A series expansion of the $\tilde{\gamma}$ function would allow us to study the asymptotic behavior for particular cases. Here we make use of Eqs. (C3) and (C4) to demonstrate numerically the dependence of the attenuation on the interaction range. From Fig. 13 it becomes clear that the DRB dominates the behavior for the intermediate regime $0<t_s<t_{12}$ also for interactions of shorter range than for dipolar interactions.

APPENDIX D: EXCITATION DENSITY VARIATION

So far we have considered the situation of spatially homogeneously distributed excitations. For the experiments on ion-doped crystals this condition is not fulfilled. From the transmission spectra in Fig. 7 it is clear that depending on the transition a considerable amount of light is absorbed by the system. Considering the Lambert-Beer law the inhomogeneity of the B-ion excitation density relative to the A-ion density is evident. Furthermore, transverse to the propagation, the laser intensity is not homogeneous either; usually the laser intensity is considered to be Gaussian distributed transverse to the direction of propagation.

To see the primary effect of the density variations, we account for two approximations. We concentrate solely on the dephasing by EFS's and we assume that density variations are negligible on scales given by the range of significant interactions leading to EFS's. Thus the averaging over the configurations of excited environments and over the long-range excitation density variations can be taken independently. Based on Eq. (20), we write

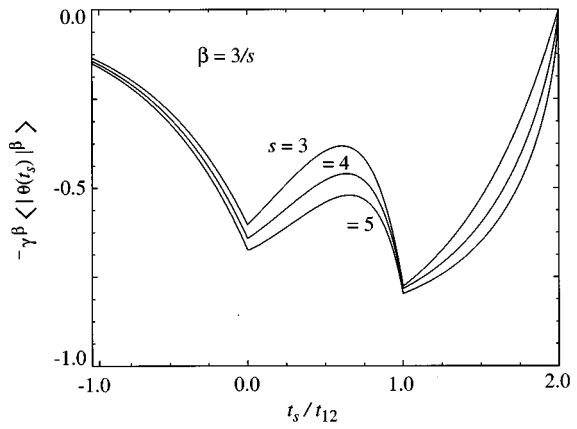

FIG. 13. Echo attenuation for different multipolar interaction ranges s. Plotted is $-\gamma^{\beta}\langle|\theta(t_s)|^{\beta}\rangle$ of Eq. (C4) for $\gamma t_{12}=1.5$, where the s values are as indicated.

$$R(t_{12},t_s)\simeq\left\langle \exp\left[-\left\langle 4\rho_0\pi p\int_0^{\infty}dr\ r^2 \times\{1-\exp[i\epsilon_0(r_0/r)^3\kappa\theta(t_s)]\}\right\rangle_{\Omega,t_f}\right]\right\rangle_p, \tag{D1}$$

where the average is taken over the density variations. Equation (D1) can be cast into

$$R(t_{12},t_s)\simeq\int dp\ \rho(p)\exp(-pG), \tag{D2}$$

where $\rho(p)$ denotes the A-ion excitation density weighted B-ion excitation density, as will become clear below and where

$$G=C_1\langle|\theta(t_s)|\rangle_{t_f}+iC_2\langle\theta(t_s)\rangle_{t_f}, \tag{D3}$$

with C_1 of Eq. (21) and C_2 of Eq. (B5). For completeness we also give

$$\gamma\langle\theta(t_s)\rangle_{t_f}=\begin{cases}(1-e^{-t_{12}\gamma})^2e^{t_s\gamma}, & t_s\leq 0\\ 1-2e^{-(t_{12}-t_s)\gamma}+e^{-(2t_{12}-t_s)\gamma}, & 0<t_s\leq t_{12}\\ e^{-(2t_{12}-t_s)\gamma}-1, & t_{12}<t_s\leq 2t_{12}.\end{cases} \tag{D4}$$

First we assume that the density p of scrambler excitations follows a Gaussian distribution

$$\rho(p)\sim\exp[-(p-\overline{p})^2/2\sigma^2], \tag{D5}$$

where $\overline{p}$ denotes the mean value of the concentration and σ is the standard deviation. Averaging gives

$$R(t_{12},t_s)\simeq\frac{\int_0^{\infty}\exp[-pG-(p-\overline{p})^2/(2\sigma^2)]dp}{\int_0^{\infty}\exp[-(p-\overline{p})^2/(2\sigma^2)]dp}. \tag{D6}$$

For $\sigma\ll\overline{p}$ the lower integration limit can be shifted to $-\infty$. Integration then yields

$$R(t_{12},t_s)\simeq\exp(-\overline{p}G+\sigma^2G^2/2), \tag{D7}$$

which corresponds to the second-order cumulant expansion. It shows a progressive effect: the larger is the absolute value of G the more the attenuation is weakened. We also note that the scaling property is lost so that the corresponding $\ln[\mathcal{I}(t_{12},t_s)/\mathcal{I}_0]/p$ data for different excitation densities p do not collapse on a single curve anymore. It turns out that the Gaussian density variation is instructive to see how the echo attenuation is influenced by weak excitation-density fluctuations.

We now consider the case of a Gaussian spatial laser intensity distribution transverse to the propagation of light. For this situation we find

$$R(t_{12},t_s)\sim\int_0^\infty dr\ r^2 e^{-(r^2/2\sigma_A^2)}\exp(-p_{B0}e^{-(r^2/2\sigma_B^2)}G), \tag{D8}$$

where p_{B0} denotes the B-ion concentration at the center of the distribution and σ_A and σ_B are the standard deviations of the transverse laser intensity distributions of the echo inducing and the scrambler laser, respectively. A concentric geometry of the two lasers is supposed. The first Gaussian in the integrand gives the density of A ions experiencing the corresponding density of B ions, which is also Gaussian distributed. By rearranging the variables we reproduce the structure of Eq. (D2), but with the density $\rho(p)$ given as

$$\rho(p)=\begin{cases} Np^{\alpha-1}\sqrt{\ln(p_{B0}/p)}, & 0<p<p_{B0} \\ 0, \quad \text{otherwise}, \end{cases} \tag{D9}$$

where

$$\alpha=\sigma_B^2/\sigma_A^2, \quad N^{-1}=\sqrt{\pi}p_{B0}^{\alpha}/(2\alpha^{3/2}). \tag{D10}$$

For $\alpha=1$, $\rho(p)$ shows a logarithmic divergence for $p\to 0$. We are not aware of an analytical solution of the integration over p so that we have to resort to numerical procedures. Numerical results are shown in Fig. 14 for $\alpha=\frac{3}{2}$. The inset shows the corresponding density $\rho(p)$; we notice a broad distribution of p values. Despite this broadness the attenuation behavior is similar to that of the homogeneous situation. We have observed a similar behavior for density variations along the propagation of the excitation pulses making use of Lambert-Beer law.[52]

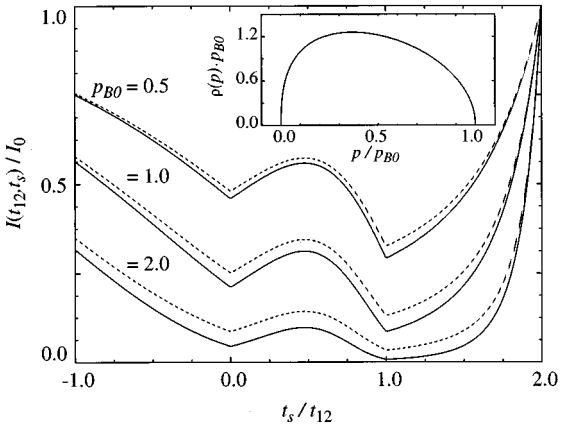

FIG. 14. Echo attenuation for a transverse Gaussian laser intensity distribution. $\mathcal{I}(t_{12},t_s)/\mathcal{I}_0$ calculated from Eqs. (3), (C3), and (C4) is plotted as dashed lines, where the p values are as indicated. Further parameters are set: $\hat{d}_A\perp\hat{d}_B$, $\epsilon_0\rho_0 r_0^3\gamma^{-1}=1$, $\alpha=(\sigma_B/\sigma_A)^2=\frac{3}{2}$, and $\gamma t_{12}=1$. For comparison also the homogeneous case is given as a full line according to Eqs. (3) and (20) with $p=\overline{p}$, where $\overline{p}$ is the first moment of the distribution $\rho(p)$, Eq. (D9), which is shown in the inset.

In conclusion, we have found that the pattern due to the DRB is robust against various modifications of the model. The DRB dominates the behavior in the intermediate regime $0<t_s<t_{12}$ also for short-range interactions and depends only weakly on moderate spatial density inhomogeneities. This makes the DRB effect very appropriate for the identification of dephasing by EFS's.

[1] J. L. Black and B. I. Halperin, Phys. Rev. **16**, 2879 (1977).
[2] J. R. Klauder and P. W. Anderson, Phys. Rev. **125**, 912 (1962).
[3] W. B. Mims, Phys. Rev. **168**, 370 (1968).
[4] S. Lyo, Phys. Rev. Lett. **48**, 688 (1982); in *Organic Molecular Aggregates*, edited by P. Reineker, H. Haken, and H. C. Wolf, Springer Series in Solid State Sciences Vol. 49 (Springer, Berlin, 1982), p. 215.
[5] D. L. Huber, J. Lumin. **36**, 307 (1987).
[6] P. Hu and L. R. Walker, Phys. Rev. B **18**, 1300 (1978).
[7] P. Hu and S. R. Hartmann, Phys. Rev. B **9**, 1 (1974).
[8] Y. S. Bai and M. D. Fayer, Phys. Rev. B **39**, 11 066 (1989).
[9] A. Suarez and R. Silbey, Chem. Phys. Lett. **218**, 445 (1994).
[10] P. Neu and A. Würger, Europhys. Lett. **29**, 561 (1995).
[11] R. M. Shelby and R. M. Macfarlane, Phys. Rev. Lett. **45**, 1098 (1980); R. M. Macfarlane and R. M. Shelby, Opt. Commun. **39**, 169 (1981).
[12] G. K. Liu, M. F. Joubert, R. L. Cone, and B. Jacquier, J. Lumin. **38**, 34 (1987); G. K. Liu and R. L. Cone, Phys. Rev. B **41**, 6193 (1990).
[13] J. Huang, J. M. Zhang, A. Lezama, and T. W. Mossberg, Phys. Rev. Lett. **63**, 78 (1989); J. Lumin. **45**, 392 (1990); J. Huang, J. M. Zhang, and T. W. Mossberg, Opt. Commun. **75**, 29 (1990); J. Zhang and T. W. Mossberg, Phys. Rev. B **48**, 7668 (1993).
[14] S. Kröll, E. Y. Xu, M. K. Kim, M. Mitsunaga, and R. Kachru, Phys. Rev. B **41**, 11 568 (1990); S. Kröll, E. Y. Xu, and R. Kachru, *ibid.* **44**, 30 (1991).
[15] M. Mitsunaga, T. Takagahara, R. Yano, and N. Uesugi, Phys. Rev. Lett. **68**, 3216 (1992).
[16] S. B. Altner, U. P. Wild, and M. Mitsunaga, Chem. Phys. Lett. **237**, 406 (1995).
[17] S. B. Altner, G. Zumofen, U. P. Wild, and M. Mitsunaga, Phys. Rev. Lett. **76**, 1747 (1996).
[18] R. M. Macfarlane and R. M. Shelby, in *Spectroscopy of Solids Containing Rare Earth Ions*, edited by A. A. Kaplyanskii and R. M. Macfarlane (North-Holland, Amsterdam, 1987).
[19] Y. P. Wang and R. S. Meltzer, Phys. Rev. B **45**, 10 119 (1992).
[20] A. J. Meixner, C. M. Jefferson, and R. M. Macfarlane, Phys. Rev. B **46**, 5912 (1992).
[21] Y. S. Bai and R. Kachru, Phys. Rev. B **46**, 13 735 (1992).
[22] G. K. Liu, R. L. Cone, M. F. Joubert, B. Jacquier, and J. L. Skinner, J. Lumin. **45**, 387 (1990).
[23] R. W. Equall, Y. Sun, R. L. Cone, and R. M. Macfarlane, Phys. Rev. Lett. **72**, 2179 (1994).
[24] R. Yano, M. Mitsunaga, and N. Uesugi, Opt. Lett. **16**, 1884 (1991).
[25] D. E. Cooper, R. W. Olson, and M. D. Fayer, J. Chem. Phys. **72**, 2332 (1980).
[26] P. Hu, R. Leigh, and S. R. Hartmann, Phys. Lett. **40A**, 164 (1972).

[27] R. M. Shelby, R. M. Macfarlane, and R. L. Shoemaker, Phys. Rev. B **25**, 6578 (1982).
[28] D. R. Taylor and J. P. Hessler, Phys. Lett. **50A**, 205 (1974).
[29] W. S. Warren and A. H. Zewail, J. Phys. Chem. **85**, 2309 (1981); J. Chem. Phys. **78**, 2298 (1983).
[30] L. Root and J. L. Skinner, J. Chem. Phys. **81**, 5310 (1984); Phys. Rev. B **32**, 4111 (1985).
[31] R. M. Macfarlane and R. S. Meltzer, J. Phys. (Paris) Colloq. **46**, C7-253 (1985).
[32] R. F. Loring and S. Mukamel, Chem. Phys. Lett. **114**, 426 (1985).
[33] *Principles of Nonlinear Optical Spectroscopy*, edited by S. Mukamel (Oxford University Press, New York, 1995).
[34] A. Blumen, J. Klafter, and G. Zumofen, in *Optical Spectroscopy of Glasses*, edited by I. Zschokke (Reidel, Dordrecht, 1986), p. 199, and references therein.
[35] P. D. Reilly and J. L. Skinner, J. Chem. Phys. **101**, 959 (1994); **101**, 965 (1994).
[36] *Theory of Molecular Excitons*, edited by A. S. Davydov (Plenum, New York, 1971).
[37] *Handbook of Stochastic Methods for Physics, Chemistry and Natural Sciences*, edited by C. W. Gardiner (Springer, Berlin, 1985).
[38] *Nonequilibrium Phonons in Nonmetallic Crystals*, edited by W. Eisenmenger and A. A. Kaplyanskii, Modern Problems in Condensed Matter Sciences Vol. 16 (Elsevier, Amsterdam, 1986).
[39] D. E. McCumber and M. D. Sturge, J. Appl. Phys. **34**, 1682 (1963).
[40] W. M. Yen, W. C. Scott, and A. L. Schawlow, Phys. Rev. A **136**, 271 (1964).
[41] L. E. Erikson, Phys. Rev. B **19**, 4412 (1979).
[42] A. A. Kaminskii, *Laser Crystals* (Springer, Berlin, 1981).
[43] M. Mitsunaga and N. Uesugi, J. Lumin. **48/49**, 459 (1991).
[44] R. W. Equall, R. L. Cone, and R. M. Macfarlane, Phys. Rev. B **52**, 3963 (1995).
[45] F. Graf, M. Mitsunaga, and U. P. Wild (unpublished).
[46] G. Zumofen and J. Klafter, Chem. Phys. Lett. **219**, 303 (1994).
[47] B. B. Mandelbrot, *The Fractal Geometry of Nature* (Freeman, New York, 1982).
[48] J. Klafter, G. Zumofen, and M. F. Shlesinger, in *Chaos, the Interplay between Stochastics, Classics, and Quanta*, edited by P. Garbaczewski, M. Wolf, and A. Weron (Springer, Berlin, 1995).
[49] D. L. Orth, R. J. Marshal, and J. L. Skinner, J. Phys. Condens. Matter **5**, 2533 (1993).
[50] W. J. C. Grant and W. M. P. Strandberg, Phys. Rev. A **235**, 715 (1964).
[51] *Tables of Integrals, Series, and Products*, edited by I. S. Gradshteyn and I. M. Ryzhik (Academic, New York, 1980).
[52] S. B. Altner, Ph.D. thesis, ETH-Zürich, 1996.